Structural Eng. / Earthquake Eng. Vol. 4. No. 2, 391s-400s. October 1987
Japan Society of Civil Engineers (Proc. of JSCE No. 386/I-8)

EARTHQUAKE SOURCE CHARACTERISTICS INFERRED FROM THE STATISTICALLY ANALYZED SPECTRA OF STRONG MOTIONS WITH AID OF DYNAMIC MODEL OF FAULTING

*By Makoto KAMIYAMA**

Response spectra of strong-motion accelerograms obtained in Japan were dealt with statistically using a multiple regression technique and the spectra at a rock site were scaled in terms of earthquake magnitude. Papageorgiou and Aki's model was considerd as an useful inhomogenous faulting model to explain the spectra. After incorporating the theoretical spectra due to the model with the statistical ones, a scaling law for the paramerers of inhomogeneous fault was derived. It was shown that the localized crack radius of inhomogeneous fault increases with earthquake magnitude M, giving a size of about 1 km for $M=6$ and about 11 km for $M=8$, and the total number of the cracks on the fault is camparatively stable irrespective of M, namely, it ranges from 10 to 20 at most between $M=6$ and $M=8$.

Keywords: earthquake fault, strong motion, statistical analysis

1. INTRODUCTION

It has been well recognized that earthquake ground motions result primarily from the three factors, namely, source characteristics, propagation path of waves, and local soil layers. Among the three factors, source characteristics have been represented approximatedly by earthquake magnitude on account of practical use in engineering. Actually, however, source mechanism is too complicated to express merely in terms of earthquake magnitude. It would be necessary to deal with such a further realistic source model as faulting even in earthquake engineering to estimate ground motions more precisely.

As for study about faulting source, Hartzell[1] proposed a skillful technique in which earthquake ground motions are estimated by taking not only faulting source but also the other factors into consideration. Hartzell's technique is a semi-empirical method since a seismogram observed during a small earthquake is used as a kind of Green function for the faulting source of an objective large earthquake. Although he originally employed the technique to estimate the ground displacement motions of periods over some seconds, it has also been recently applied in engineering field, where acceleration motions consisting mainly of periods less than some seconds are discussed about, because of its utility[2]. The estimation of acceleration motions, however, has not been yet conducted satisfactorily because the principle for superposing small earthquake records with regard to the faulting is not so valid as for the case of the displacement motions. Finding the inhomogeneous characteristics of faulting which stimulate acceleration motions, therefore, would be an important key to carry out the technique with success in engineering field. The objective of this study is to make clear some aspects of inhomogeneous faulting source to answer the above requirement.

* Member of JSCE, Dr. Eng. Associate Professor, Dept. of Civil Eng., Tohoku Institute of Technology (Yagiyama-kasumicho, Sendai 983, Japan)

Since earthquakes generally occur in deep regions of crust with a complicated manner, it would be impossible to seize directly the details of their mechanism. The first step to attack such complicated phenomena may be a rough estimation based on indirect methods. From this point of view, the present study deals with rather rough understanding of inhomogeneous faulting by use of a statistical analysis of strong-motion accelerograms.

2. STATISTICAL ANALYSIS OF STRONG-MOTION SPECTRA

Acceleration spectra are fundamental in earthquake engineering. In addition, Fourier spectra are ideal to investigate precisely the relation between spectra and source parameters. Thus Fourier acceleration spectra are required in this study. But, in spite of this required condition, Fourier spectra are hard to treat in the points of the analyzed interval of records and smoothing problem. Luckily, on the other hand, velocity response spectra having no damping ($h=0$, h : damping ratio) are nearly equal to Fourier acceleration spectra and give the upper limited values for them, and also are calculated with less difficulty[3]. For these reasons, the present study uses velocity response spectra ($h=0.0$) instead of Fourier spectra in order to investigate source characteristics.

(1) A statistical model for analyzing strong-motion spectra

Earthquake ground motions are mainly influenced by source characteristics, propagation path of waves, and local soil layers as described above. The author proposed a statistical model, as follows, for quantitatively separating the effects due to the three factors from the strong-motion spectra observed at the ground surface[4].

$$\log_{10} V(T)=a(T)M+b(T)\log_{10}(\Delta+30)+c(T)D+d(T)+\sum_{i=1}^{N-1}A_i(T)S_i, \quad \cdots\cdots (1)$$

where V : response spectra, M : earthquake magnitude, Δ : epicentral distance, D : focal depth, S_i : dummy variable, $a(T)$, $b(T)$, $c(T)$, $d(T)$, $A_i(T)$: regression coefficients, T : period, and N : total number of observation sites.

Although Eq. (1) is such a simplified model that the above each factor is expressed merely in terms of earthquake magnitude, epicentral distance, focal depth, and dummy variables, it is very useful to predict response spectra at a given site. The detailed derivation and physical meaning for the model were described fully in Ref. 4. Here, to analyze the source characteristics in more detail, the following expression is given by adding the power term of magnitude M to Eq. (1) :

$$\log_{10} V(T)=a(T)M^2+b(T)M+c(T)\log_{10}(\Delta+30)+d(T)D+e(T)+\sum_{i=1}^{N-1}A_i(T)S_i. \quad \cdots\cdots (2)$$

The power term of magnitude M was included in Eq. (2) for the two reasons, namely, one is that higer order terms generally make the regression expression more precise and the other that earthquake parameters are considered to be not linear against magnitude M as pointed out by Geller[16].

We use Eq. (2) as a statistical tool for deriving a scaling law of source spectra below.

(2) Strong motion accelerograms used for the statistical analysis

The statistical model of Eq. (2) was applied to the same strong-motion accelerograms described in Ref. 4. These are composed of 228 horizontal accelerograms having maximum acceleration more than 20 gal[5),6)]. The observation sites and earthquake origins for these accelerograms are indicated in Fig. 1. As shown in Fig. 1, the observation sites are 26 in all, and these accelerograms were obtained on the conditions that earthquake magnitude M ranges from 4.1 to 7.9 (mean=6.4), epicentral distance Δ from 3 to 350 km (mean=77.7 km), and focal depth D from 0 to 130 km (mean=43 km).

The above accelerograms were caught mostly by the SMAC types of accelerographs. As well known, many numerical errors due to frequency characteristics of instrument, digitization processing and so on are involved in the digitized accelerograms. Of these errors, the instrument one was removed by performing the frequency characteristics correction according to each accelerograph. Further, the other

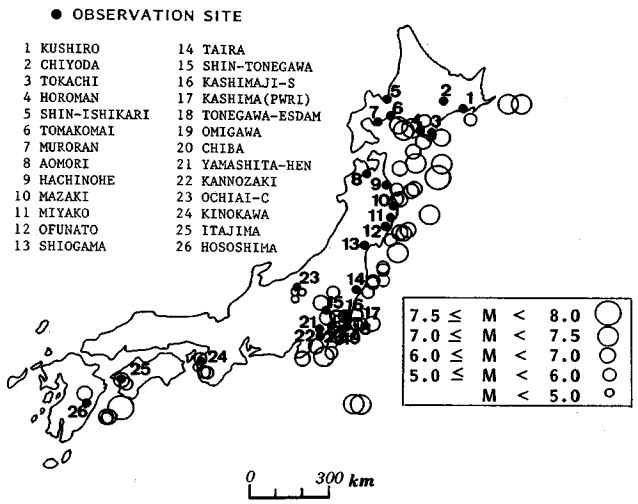

Fig. 1 Map showing observation sites and earthquake origins.

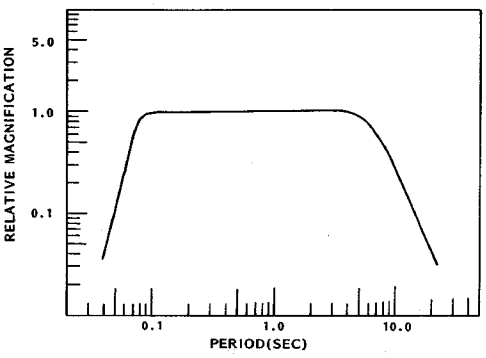

Fig. 2 Overall frequency characteristics of the low pass filer and high pass filer.

errors, especially, in higher and lower frequency domains were eradicated through the low pass filer and high pass filer proposed by Iai et al[7]. The overall frequency characteristics of the both filters are shown in Fig. 2. Fig. 2 indicates that the spectra used here must be discussed about within the flat part of periods ranging from about 0.09 sec to about 4.2 sec. The limited period band should be emphasized, in particular, when the so-called corner frequency of spectra is examined.

(3) Statistical analysis results and averaged source spectra

Velocity response spectra with no damping (h=0.0) were calculated from the accelerograms mentioned above, and were statistically analyzed in accordance with Eq. (2). In the statistical analysis, as explained in Ref. 4), it is needed to pick up one site from all the observation sites as a base site for obtaining amplification factors due to individual local site condition with physical meaning. We selected OFUNATO site, which is labeled 12 in Fig. 1, as the base site for the same reason described in Ref. 4. We can find very rigid slate at OFUNATO site and its S-wave velocity is inferred from many geological materials to be about 1~2 km/sec even though no exact measurement has been carried out. Accordingly, $V(T)$ estimated by using the first five terms exept the sixth of the right hand side in Eq. (2) means the response spectra at a rock site having such a rigidity. Here, it should be noted that these rock site spectra are represented as ones on outcrop surface in order to compare them with the free surface spectra will be theoretically derived in the later section, whereas they were given as incident motion spectra into underlying bed rock in Ref. 4.

The regression coefficients $a(T)$, $b(T)$, $c(T)$, $d(T)$ and $e(T)$ resulting from the statistical analysis of Eq. (2) are given in Fig. 3. On the other hand, the coefficients, $A_i(T)$ (i=1~N−1) which signify the amplification factors of spectra for each observation site were gotten as the values almost similar to the ones of Eq. (1). In this paper, we are interested in the rock site spectra in connection with earthquake source rather than the amplification factors owing to individual site condition, so the results of $A_i(T)$ are not shown here. The regression coefficients shown in Fig. 3 make it possible to estimate the velocity response spectra (h=0.0) at the rock site according to Eq. (2) provided that M, Δ and D are available. Fig. 4 presents the rock site spectra which were estimated varying earthquake magnitude while keeping epicentral distance and focal depth constant (Δ=77.7 km, D=43 km). Since these constant distance and depth are equal to the mean values of each parameter used in the statistical analysis, Fig. 4 can be understood as the source spectra which are normalized statistically by the mean values of epicentral distance and focal depth and moreover are scaled in terms of earthquake magnitude. In other words, Fig. 4 would be regarded as a kind of scaling law of the source spectra deduced statistically from the past

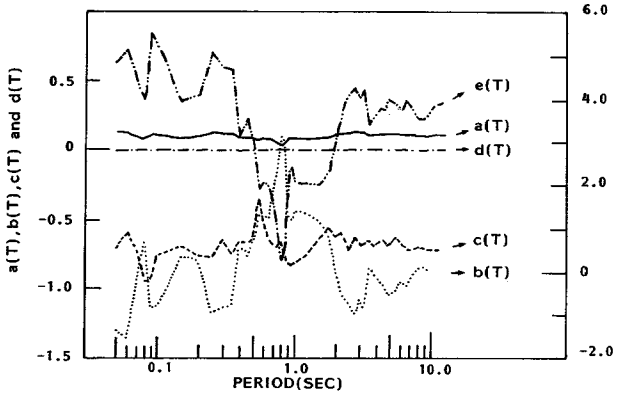

Fig. 3 Regression coefficients of the statistical analysis.

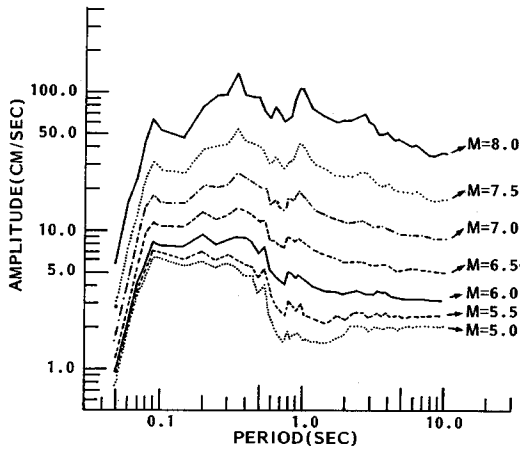

Fig. 4 Rock site spectra statistically scaled with earth quake magnitude (Δ=77.7 km, D=43 km).

strong-motion accelerograms.

Fig. 4 reveals the facts that there seems to be two corner periods in short and long period domains even though a little different trend is found according to magnitude M, and that the spectra have nearly flat configurations between the two corners. In addition to being almost the same values around 0.09 sec irrespective of magnitude M, the shorter corner periods are nearly equal to the shorter cutoff period in Fig. 2. Hence the shorter corner periods here would be owing to the low pass filter applied to the accelerograms. As for corner period of spectra, Hanks[8] discussed about a higher corner frequency f_{max} in acceleration spectra. To discuss about f_{max} here, we need more wide-ranged spectra, especially, in shorter period domain, but such discussion is beyond our urgent aims. The longer corner periods, on the other hand, exist around 0.5 sec for the magnitudes of M=5 or M=6, and seem to become longer as magnitude increases. In addition, the existence of the longer corner periods becomes rather invalid together with larger magnitude. In any case, the spectra shown in Fig. 4 may reflect the characteristics peculiar to source mechanism.

3. THEORETICAL SOURCE SPECTRA BY A DYNAMIC MODEL OF FAULTING

It is almost impossible for the conventional faulting model like Haskell's one[9] to explain such high spectral amplitude in shorter period domain as shown in Fig. 4. This drawback to the conventional models has lead to the recent inhomogeous faulting models which have non-uniform parameters on their fault planes so that acceleration waves are more strongly originated in shorter period domain[10]. Although several heterogeneous faulting models have been presented by many researchers to explain the strong radiations of acceleration waves, the so-called specific barrier model by Papageorgiou and Aki[11] is not only comparatively simple but also easy to understand physically. Furthermore it can effectively offer the expected values of source spectra. Thus this model can satisfy our requirments, and it is adopted as the theoretical model to explain our statistical spectra.

Papageorgiou and Aki considered such an idealized rectangular faulting model with the sizes of length L and width W as illustrated in Fig. 5. Their model consists of the localized circular cracks with constant radius ρ_0, which are assumed to slip according to the manner modeled by Sato and Hirasawa[12], and barriers distributed over the fault plane. Although they derived the expected values of acceleration power spectra, we examine here the expected values of acceleration Fourier spectra due to the model for the comparison of the empirically obtained spectra in Fig. 4.

Suppose now that a potential circular crack subject to stress $\Delta\sigma$ was placed in the uniformly

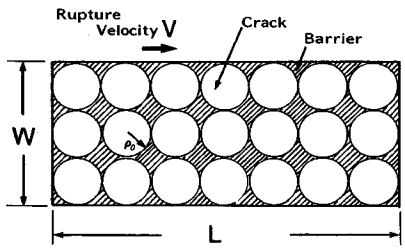

Fig. 5 Papageorgiou and Akis faulting model.

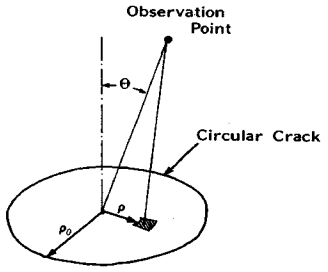

Fig. 6 Circular crack fault model.

homogeneous medium as shown in Fig. 6. Following Sato and Hirasawa, and/or Papageorgiou and Aki, when the slip starting at the center of the circular crack propagates outward and stops suddenly on the circumference, the acceleration Fourier spectrum $|A_0(\omega)|$ in a far-field point ($\theta \neq 0$) is given by, on condition of cancelling geometric spreading

$$|A_0(\omega)| = \left(\left\{ a_1 t_1 \frac{\sin X}{X} - a_2 (t_2 - t_1) \frac{\sin Y}{Y} \cos \frac{\omega t_2}{2} - (a_1 + a_2) t_1 \cos \frac{\omega t_1}{2} + a_2 t_2 \cos \left(\omega t_2 - \frac{\omega t_1}{2} \right) \right\}^2 \right.$$
$$\left. + \left\{ a_2 (t_2 - t_1) \frac{\sin Y}{Y} \sin \frac{\omega t_2}{2} + (a_1 + a_2) t_1 \sin \frac{\omega t_1}{2} - a_2 t_2 \sin \left(\omega t_2 - \frac{\omega t_2}{2} \right) \right\}^2 \right)^{1/2}, \quad \cdots\cdots (3)$$

where $X = \omega t_1/2$, $Y = \omega(t_2 - t_1)/2$, $t_1 = \rho_0(1-k)/v$, $t_2 = \rho_0(1+k)/v$, $a_1 = 4Kv^3\pi/(1-k^2)^2$, $a_2 = Kv^3\pi/k(1+k)^2$, $k = v \sin\theta/\beta$, $K = 24\,\Delta\sigma/(7\,\pi\mu)$,

v : propagation velocity of slip, β : shear wave velocity, μ : rigidity modulus, and ω : circular frequency.

We can get the expected value for $|A_0(\omega)|$ over the focal sphere by using the following expression :

$$\langle |A_0(\omega)| \rangle = \int_0^{\pi/2} |A_0(\omega)| \sin\theta d\theta, \quad \cdots\cdots (4)$$

where $\langle |A_0(\omega)| \rangle$ is the expected value of $|A_0(\omega)|$.

For example, the expected value $\langle |A_0(\omega)| \rangle$ is estimated as drawn in Fig. 7 on the conditions of $\beta =$ 3.5 km/sec and $v = 2.52$ km/sec which satisfy Geller's expression[16] $v/\beta = 0.72$. In Fig. 7, the value of $\langle |A_0(\omega)| \rangle$ normalized by $\pi K v^2 \rho_0$ is plotted against the period normalized by ρ_0/v. It is found in Fig. 7 that the acceleration spectrum due to this crack model resembles relatively well the statistical ones in Fig. 4, giving almost flat configuration in the period range shorter than a corner period which is considered to be equivalent to the larger corner period mentioned in 2. Fig. 7 also indicates that the spectral amplitude is large in shorter period range, and then we examine the asymptotic form of $\langle |A_0(\omega)| \rangle$ for large ω in the following.

Consider here a simplified rectangular fault where the above described circular cracks and barriers are distributed uniformly as shown in Fig. 8. Although the slips owing to each crack spread successively from one to another, earthquake waves radiated by their stopping phases[11] are supposed to arrive incoherently at a point far from the fault. With such incoherency and the radition pattern due to shear dislocation, we can derive the expected value $\langle |F(\omega)| \rangle$ for horizontal acceleration Fourier spectrum at a point, which has free surface and is r_0 away from the center of the fault, as follows :

$$\langle |F(\omega)| \rangle = \frac{2}{\sqrt{2}} \frac{R^s}{4\pi\beta r_0} \cdot \sqrt{S} \left(\pi \frac{\Delta u'_{\max}}{\rho_0} \right) v\beta C, \quad \cdots\cdots (5)$$

where R^s : radiation pattern peculiar to shear dislocation, $S = L \times W$ (fault area), r_0 : distance from the center of the fault to the point, $\Delta u'_{\max}$: local maximum dislocation of each crack, ρ_0 : radius of each crack, and

$$C = \frac{1}{\sqrt{2}} \int_0^{\pi/2} \frac{\sqrt{1+k^2}}{1-k^2} d\theta,$$

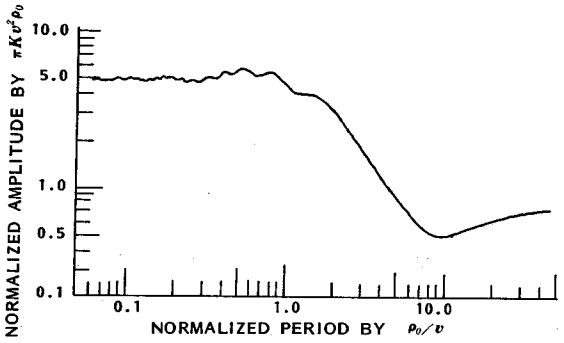

Fig. 7 Expected value of far-field Fourier spectra of acceleration.

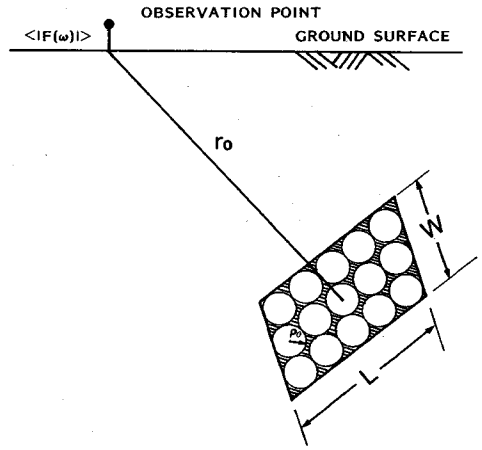

Fig. 8 Schematic profile of faulting model and observation point.

where $k=v\sin\theta/\beta$.

In Eq. (5) we replaced the stress drop $\Delta\sigma$ with the local maximum dislocation $\Delta u'_{max}$ for the sake of convenience, and the constants 2 and $1/\sqrt{2}$ are terms caused by the so-called surface amplification and vectorial partition of motions, respectively.

4. SOURCE CHARACTERISTICS INFERRED FROM THE COMPARISON BETWEEN THE STATISTICAL SPECTRA AND THEORETICAL ONES

Eq. (5) makes it possibles to predict $\langle|F(\omega)|\rangle$ provided that some fault parameters like S, ρ_0, and so on are available. Speaking conversely, however, it is also an expression to estimate the fault parameters from $\langle|F(\omega)|\rangle$. As explained previously, the spectra in Fig. 4 correspond to the $\langle|F(\omega)|\rangle$ statistically scaled with earthquake magnitude M. Therefore, it follows that we can obtain how the unknown parameter ρ_0 is scaled with M by combining the spectra in Fig. 4 with Eq. (5).

In the above discussion, it is an important problem whether or not the spectra in Fig. 4 are composed of shear waves, since Eq. (5) was derived from only shear waves. By the way, Hanks[13] and Kamiyama[14] showed individually that shear waves dominate in shorter periods than about 1~2 sec, whereas surface waves are predominant in periods longer than that. As will be shown later, the spectral amplitudes in Fig. 4 are dealt with almost within such period range of shear waves. So this suggests that there is little difference in waves between Eq. (5) and Fig. 4.

Among the parameters involved in Eq. (5), the fault area and maximum dislocation of faulting were relatively well revealed from the past many earthquakes and they have been associated empirically with earthquake magnitude. Here, referring to the empirical expression presented by Sato[15], the following expressions are obtained:

$$\sqrt{S}=10^{0.5M-2.04}, \quad (6)$$

$$\Delta u'_{max}=\frac{6}{\pi}10^{0.5M-1.4}. \quad (7)$$

Eq. (7) was derived with aid of the following relation[11] between the local maximum dislocation $\Delta u'_{max}$ in the barrier model and the averaged dislocation $\overline{\Delta u}$ in the global faulting model as well as Sato's $\overline{\Delta u}$-M relations,

$$\Delta u'_{max}=\frac{6}{\pi}\overline{\Delta u}. \quad (8)$$

The substitution of Eqs. (6) and (7) into Eq. (5) gives

$$\rho_0=\left(\frac{2}{\sqrt{2}}\frac{R^s}{4\pi r_0}6\,vC\,10^{M-3.44}\right)/\langle|F(\omega)|\rangle. \quad (9)$$

We can estimate the values of ρ_0 varied according to M by using Eq. (9) as well as the spectra in Fig. 4. In order to do so, we further need the constants R^s, β, v and r_0 appropriate for the spectra in Fig. 4. These constants are determined as follows.

The Fourier spectra $\langle|F(\omega)|\rangle$ in Fig. 4 were obtained through the statistical dealing of the accelerograms from many observation sites distributed at random around various types of earthquakes as described previously. That is, the averaged radiation pattern between various sources and observation points may be proper to the present spectra. Thus R^s is assigned to be 0.63 which is the expected value of the radiation pattern on the focal sphere for shear dislocation. On the other hand, the statistical spectra in Fig. 4 were also given as the spectra at the outcrop having shear wave velocity of 1~2 km/sec as well as due to the earthquake origin of focal depth D=43 km. It would be quite difficult to allot an adequate shear wave velocity for such origin and observation site, but its precise value may be meaningless if we consider the degree of roughness for the other parameters. In the present case, accordingly, β=3.5 km/sec is assumed in consideration of the averaged shear wave velocity of the crust around Japan. According to this assumption, v is set to be 2.52 km/sec using Geller's expression v/β=0.72[16]. Also r_0=88.8 km was conditioned because the spectra in Fig. 4 were obtained as Δ=77.7 km and D=43 km.

The above constants and Eq. (9) result in Table 1 after calculating the average spectral amplitudes in the high level parts of each spectrum in Fig. 4 and substituting them to Eq. (9). In Table 1, the mean and standard deviation for $\langle|F(\omega)|\rangle$ and ρ_0 are tabulated together with the period range for averaging the spectral amplitudes. In addition, the mean value and standard deviation of the total crack numbers, which are obtained by using ρ_0-S relations, are also shown in Table 1. The period ranges for the averaged spectral amplitude were determined in accordance to each magnitude M, considering the frequency characteristics of the filter shown in Fig. 2 as well as the level and flatness of the spectral amplitudes.

The crack radius ρ_0 and total crack number n in Table 1 are plotted against the variations of M in Figs. 9 and 10, respectively. We can see from Table 1 and Fig. 9 that the radius of localized crack increases with earthquake size, having about 1.0 km for M=6 and about 11 km for M=8. From Fig. 9 and Table 1, the regression expression between the radius ρ_0 and earthquake magnitude M is given by

$$\rho_0=10^{0.63M-3.87}. \quad (10)$$

From Table 1 and Fig. 10, on the other hand, the total crack number n of faulting appears to be minimum around M=7, while it gets larger with decreasing magnitude and slightly larger with increasing magnitude. The increasing trend of the total crack number is emphasized especially in smaller magnitudes than 6. As mentioned above, the total crack number here was estimated by using the empirical relations of S-M in Eq. (6) as well as the values of ρ_0 in Table 1. However, fault area S of earthquake may be less reliable in such small magnitudes because of the difficulty of estimation even though any kinds of empirical relations for S-M are employed. For this reason, it should be further examined after due consideration whether the characteristics in smaller magnitude are actually valid or not. In contrast to the above trend in smaller magnitude, the total crack number n seems to be rather stable in earthquake magnitudes greater than 6. Earthquake damages, in general, are caused by such class of magnitudes, so the total crack number in the domain of M>6 would be more important from the view point of engineering. In this domain, the total crack numbers containing their statistical standard deviations are almost within the extent from 10 to 20, although there is an amount of scatter. When we consider the roughness of the present method, it would be relevant to conclude that the total crack number of faulting in such a size of earthquake as giving damages is relatively stable irrespective of magnitude and is from 10 to 20 at most or at least.

Table 1 Relations between circular crack radius, total number of cracks and earthquake magnitude.

Magnitude	5.0	5.5	6.0	6.5	7.0	7.5	8.0
Period range for $<\|F(\omega)\|>$ (sec)	0.09 ~ 0.45	0.09 ~ 0.55	0.09 ~ 0.55	0.09 ~ 0.55	0.09 ~ 1.20	0.09 ~ 1.80	0.09 ~ 4.20
$<\|F(\omega)\|>$ (cm/sec)	5.54 ±0.57	6.12 ±0.64	8.11 ±0.64	12.10 ±1.24	18.24 ±3.23	35.26 ±7.20	71.55 ±19.56
Radius of cicular crack ρ_0 (km)	0.14 ±0.02	0.41 ±0.04	0.99 ±0.08	2.09 ±0.21	4.38 ±0.78	7.17 ±1.46	11.17 ±3.05
Number of crack n	103 ±11	39 ±4	22 ±2	15 ±2	13 ±2	13 ±3	17 ±5

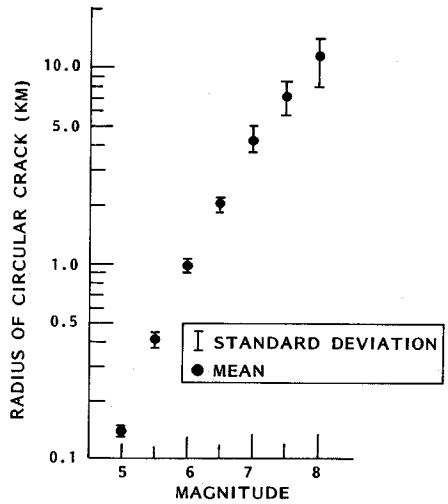

Fig. 9 Relation between the radius of circular crack and earthquke magnitude.

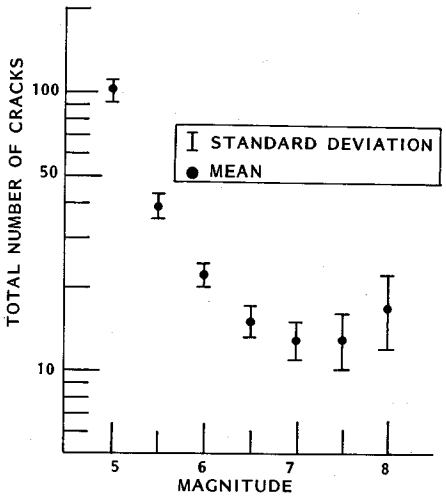

Fig. 10 Relation between the total number of cracks and earthquake magnitude.

5. INTERPRETATION OF THE ESTIMATED SOURCE PARAMETER FROM THE PAST OBSERVED DATA

As explained previously, heterogeneous faulting model recently has become to arouse researcher's interest, so the observed data about the model are still little except for Aki's data[17]. Aki obtained some values of the barrier interval of fault from the past representative earthquakes throughout the world by making use of geological materials or seismic ones. Here, Fig. 9 is compared with Aki's results in order to investigate its validity. Aki's results are plotted in Fig. 11 after arranging as ρ_0~M relation, where ● and ▲ are due to geological and seismic data, respectively. In Fig. 11 the similar relations obtained by the present study are also shown. Fig. 11 indicates that the present study is relatively compatible with Aki's results, even though there is a little difference between the both.

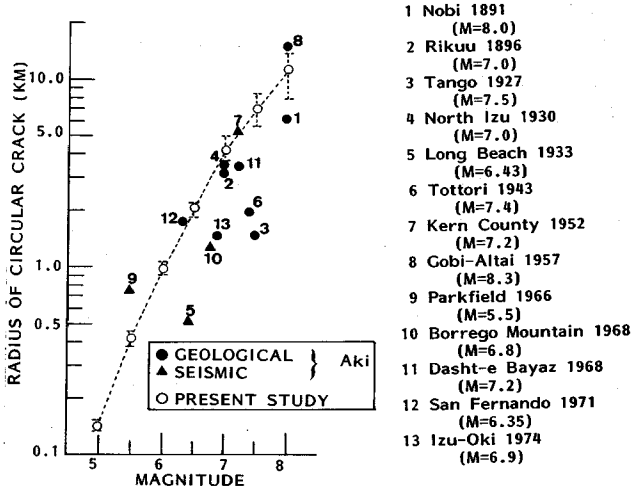

Fig. 11 Camparison between Aki's results and the present ones for the crack radius-earthquake magnitude relation.

Generally speaking, the parameters of heterogeneous fault such as ρ_0 are very difficult to exactly seize and besides Aki's results were deduced from some very old earthquakes. Hence, the compatibility between the both would not be bad if we consider such ambiguities belonging possibly to Aki's results.

It seems in Fig. 11 that the present study gives an upper band for Aki's results. The reason leading to such a trend is not clear within this study. Anyway many more precise observational data about heterogeneous faulting are required to confirm the validity of this study.

6. THEORETICAL SPECTRA ESTIMATED FROM THE PRESENT PARAMETERS OF INHOMOGENEOUS FAULT

In the preceding section, the validity of the ρ_0–M relation obtained by the present study was investigated from the comparison with other reseacher's data. Such investigation can also be carried out by an another method which makes use of spectral configuration. As shown already, the spectra due to the inhomogeneous faulting in question have a corner period, and the period is independent of the spectral amplitudes in shorter period range. Besides the inhomogeneous fault parameter ρ_0 was obtained with aid of only the spectral amplitude in shorter period range as described in 4. Therefore, it would be possible to investigate the reasonability of ρ_0 in Table 1 by comparing the corner period of the spectra estimated due to the ρ_0 with some observed ones.

In Eq. (5) only spectral amplitude in period range shorter than the corner period was formulated for simplicity. But, an another derivation from Eq. (3) can give numerical spectral amplitudes in whole period domain. By using such numerical calculation method and ρ_0 listed on Table 1 as well as the constants such as R^s, β, v and r_0 provided in 4, the theoretical spectra due to the present faulting are obtained as shown in Fig. 12. In Fig. 12 the spectra are shown for representative earthquake magnitudes. The comparison between Fig. 12 and Fig. 4 signifies that the corner periods for each magnitude in Fig. 12 coincide comparatively well with the observed longer corner periods in Fig. 4, in particular, for magnitude greater than 6, which is important in earthquake engineering, except for the case of $M=5$. It would be thus pointed out that the ρ_0–M relations obtained by the present study is reasonable even from the view point of corner period of spectra.

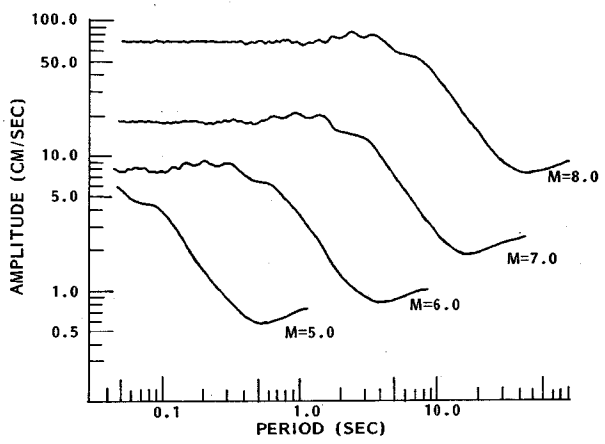

Fig. 12 Theoretical spectra due to the inhomogeneous faulting model. (M : Magnitude)

7. CONCLUDING REMARKS

The principal conclusions drawn from this study are summarized as follows.

(1) The acceleration spectra statistically obtained from the strong-motion records have nearly flat spectral configuration between the two corner periods, and the configuration can be explanined quantitatively well by the inhomogeneous faulting model of Papageorgiou and Aki.

(2) The conjuntion of the statistical spectra and the inhomogeneous faulting theory leads to a scaling law about the localized crack radius ρ_0 of inhomogeneous fault as presented in Eq. (10). According to the law, the radius increases with earthquake magnitude M, and for instance, it has a size of about 1.0 km for $M=6$ and about 11.0 km for $M=8$.

(3) The total number of cracks for inhomogeneous fault is relatively stable regardless of earthquake magnitude, particularly, in earthquake size of causing damages to structures. That is, the total crack

number is from 10 to 20 at most or at least between $M=6$ and $M=8$.

(4) The ρ_0-M relation obtained by the present study was confirmed to be consistent to the data observed geologically or seismologically during the past representative earthquakes.

(5) The corner periods of the theoretical spectra due to the inhomogeneous faulting model are comparable to the ones found in the statistical spectra from the strong-motion records.

Papageorgiou and Aki's model is such a very idealized model that individual crack distributed on the fault plane is assumed to have an equal size, and therefore rather different results may be derived if the inequality of crack size is considered. In this point, the above results should be regarded as an averaged aspect of inhomogeneous fault. Even if so limited, however, the presented results would be useful to estimate acceleration ground motions with aid of faulting source model, for example, Hartzell's method. The technique of how to incorporate the present results with the prediction of earthquake ground motions will be described in author's another paper.

REFERENCES

1) Hartzell, S.H. : Earthquake aftershocks as Green's functions, Geophys. Letters, Vol. 5, No. 1, pp. 1~4, 1978.
2) Iida, M. and Hakuno, M. : The synthesis of the accelearion wave in a great earthquake by small earthquake records, Proc. of JSCE, No. 329, pp. 57~68, 1983.
3) Hudson, D.E. : Reading and Interpretation Strong Motion Accelerograms, pp. 55~64, Earthquake Engineering Research Institute, 1979.
4) Kamiyama, M. and Yanagisawa, E. : A statistical model for estimating response spectra of strong earthquake ground motions with emphasis on local soil conditions, Soils and Foundations, Vol. 26, No. 2, pp. 16~32, 1986.
5) Tsuchida, H. et al. : Annual Report on Strong-Motion earthquake Records in Japanese Ports 1986-1983, Technical Note of the Port and Harbour Research Institute No. 98-No. 458, The Port and Harbour Research Institute, Ministry of Transport, 1969~1983.
6) Iwasaki, T. et al. : Strong-Motion Acceleration Records from Public Works in Japan No. 1-No. 8, Technical Note of the Public Works Research Institute, Vol. 32-38, The Public Works Research Institute, Ministry of Construction, 1978~1983.
7) Iai, S., Kurata, E. and Tsuchida, H. : Digitization and correction of strong-motion accelerograms, Technical Note of the Port and Harbour Research Institute, No. 286, pp. 5~56, 1978 (in Japanese).
8) Hanks, T.C. : f_{max}, Bull. Seism Soc. Am. Vol. 72, pp. 1867~1879, 1982.
9) Haskell, N.A. : Total energy spectral density of elastic wave radiation from propagating faults, Bull. Seism. Soc. Am., Vol. 54, no, 6, pp. 1811~1841, 1964.
10) Hirasawa, T. : Prediction of maximum acceleration due to a stochastic source model, Report of Special Research on National Disasters, No. A-54-3, pp. 35~45, 1979 (in Japanese).
11) Papageorgiou, A.S. and Aki, K. : A specific barrier model for the quantitative description of inhomogeneous faulting and the predition of strong ground motion, Part I and Part II, Bull. Seism. Soc. Am. Vol. 73, pp. 693~722, pp. 953~978, 1983.
12) Sato, T. and Hirasawa, T. : Body wave spectra from propagation shear cracks, J. phys. Earth. Vol. 21, pp. 415~431, 1973.
13) Hanks, T.C. : Strong ground motion of the San Fernando, California, earthquake : ground displacements, Bull. Seism. Soc. Am. Vol. 65, pp. 193~225, 1975.
14) Kamiyama, M. : A study on Strong Earthquake Ground motions with application to prediction, Doctoral thesis, Tohoku Univ., 1985 (in Japanese).
15) Sato, R. : Theoretical basis on relationships between focal parameters and earthquake magnitude, J. Phys. Earth Vol. 27, pp. 353~372, 1979.
16) Geller, R.J. : Scaling relations for earthquake source parameters and magnitudes, Bull, Seism. Soc. Am. Vol. 66, No. 5, pp. 1501~1523, 1976.
17) Aki, K. : Asperities, barries charateristic earthquake and strong motion prediction, J. Geophys. Res. Vol. 89, No. B 7, pp. 5867~5872, 1984.

(Received September 10 1986)